International Core Journal of Engineering Volume 10 Issue 5, 2024
ISSN: 2414-1895 DOI: 10.6919/ICJE.202405_10(5).0039

Effects of Curing Temperature and CO_2 Concentration on the Properties of Magnesium Slag Carbonized Blocks

Mingqiang Liu[a], Cheng Zhang[b], Ruiqi Zhao[c,*], and Xuemao Guan[d]

School of Materials Science and Engineering, Henan Polytechnic University, Jiaozuo 454003, China

[a]liumingqiang@home.hpu.edu.cn, [b]2837116601@qq.com, [c,*]zhaoruiqi@hpu.edu.cn, [d]guanxuemao@hpu.edu.cn

Abstract

During the smelting of magnesium by the Pijiang method, a large amount of magnesium slag is produced, and high-temperature flue gas with low CO_2 concentration is also emitted. Both magnesium slag and flue gas have the problem of low utilization rate. In order to improve the utilization rate of magnesium slag as well as to sequester the CO_2 produced in the process of magnesium smelting, this work reported magnesium carbonation slag products with magnesium slag as raw material under curing conditions of different temperatures and different CO_2 concentrations, and systematically investigated the effects of the curing temperature and CO_2 concentrations on the properties of magnesium carbonation slag products. The results show that the appropriate reduction of temperature is conducive to the increase of mechanical properties of the samples. Directly using high temperature and low CO_2 concentration of magnesium smelting flue gas, the compressive strength of the samples is only 17.75 MPa; when the temperature is reduced to 80 ℃, the compressive strength increased to 32.92 MPa; and as the temperature is further lowered to 25 ℃, the compressive strength is increased to 39.35 MPa. The compressive strength of the magnesium slag carbonized specimen was as high as 63.06 MPa when being cured at 25 ℃ and a CO_2 concentration of 30%. The microstructure showes that both higher temperature and lower CO_2 concentration increase the porosity and water absorption of the sample, and reduce the density of the sample, which is detrimental to the carbonization of the sample.

Keywords

Magnesium Slag; Curing Temperature; CO_2 Concentration; Compressive Strength; Pore Structure.

1. Introduction

Magnesium slag (MS) is a strongly alkaline solid waste produced during the smelting of magnesium metal [1]. The annual production of magnesium metal in China accounts for more than 85% of the global production, and a large amount of magnesium slag solid waste is generated during the production of magnesium [2]. Pijiang method is the main method of smelting magnesium in China, and 5-7 t of magnesium slag will be generated for every 1 t of magnesium metal [3]. Many smelting enterprises mainly dispose of magnesium slag by stockpiling or landfilling, and there is no effective method to utilize magnesium slag on a large scale. As of 2021, only in Yulin area, 60 million tons of magnesium slag will be disposed of [4]. The disposal of magnesium slag will cause serious environmental pollution to the soil and the surrounding areas. The raw material for the production of magnesium metal is mainly dolomite, and the process of calcining dolomite releases CO_2, and every

ISSN: 2414-1895 DOI: 10.6919/ICJE.202405_10(5).0039

1 t of magnesium produced emits 26.3 t of CO_2 [5]. Therefore, it is important to explore methods for effective disposal of magnesium slag and sequestration of CO_2.

Current research on the application of magnesium slag has focuses on the fields of soil slaking agents [6-7], desulfurizers [8-9], and construction materials [10-12]. Given the wide application of construction materials, producing building materials with magnesium slag has become an effective way of solving the problem of magnesium slag. Li et al [13] found that the use of magnesium slag as a substitute for limestone up to 30% (mass fraction) can play a role in lowering the sintering temperature of clinker. Ji et al[14] added magnesium slag as an admixture to concrete, and found that the concrete's strength decreased in the early stage but the increased significantly in the later stage. Mo et al [15] used magnesium slag to accelerate carbonation to prepare cement mortar specimens, and the compressive strength reached 119.5 MPa. Zhong et al [16] added aragonite whiskers prepared from magnesium slag to cement, and found that the addition of 5% to 20% aragonite whiskers could increase the compressive and flexural strengths of the cement in the early and late stages.

On the other hand, carbonization conditions play an important role in carbonized products[17- 18]. Lei et al[19] investigated the carbonization process of slag blocks in an oxygen converter at different temperatures (60~140 ℃) and different relative humidities (2~60%), and the results showed that the compressive strength of slag blocks increased with the increase of temperature, but when the slag blocks were carbonized at high temperatures, sufficient water vapor was essential to guarantee the strength of the blocks. Zhang et al [20] cured magnesium slag with steam and found that the carbonization of magnesium slag could reduce the stability risk. Xie et al. studied the carbonization process of cement fiberboards prepared with magnesium and found that the concentration and pressure of CO_2 had a significant effect on the specimens, and that the flexural strength of the specimens cured with 30% concentration (v/v) of CO_2 increased the fastest [21]. The effects of carbonization conditions, steam conditions, concentration and pressure of CO_2 on the properties of magnesium slag products has been reported in the literatures. However, the coupling effect of high temperatures and low CO_2 concentration of industrial flue gase has not been studied.

This paper intends to systematically study the effects of temperature and concentration of CO_2 on the physical properties of magnesium slag blocks by simulating the flue gas emitted from magnesium kilns. Magnesium slag is used as raw material. The identification of phases, changes in pore structure and micro morphology with curing temperature and CO_2 concentration will be presented in detail. These results should provide useful information for better utilization magnesium slag and reduction of CO_2 emissions.

2. Experimental Section

2.1 Raw Material

The magnesium slag was taken from Yulin City, Shaanxi Province. The chemical composition of magnesium slag is shown in Table 1, and the XRD pattern is shown in Fig. 1a. The chemical composition of the magnesium slag was expressed in the form of oxides, mainly include CaO, SiO_2, MgO, Fe_2O_3 and Al_2O_3, and the phases were mainly β-C_2S, γ-C_2S, $CaCO_3$, $Ca(OH)_2$, CaO and MgO. The magnesium slag was milled by ball mill for 15 min, and the particle size distribution of magnesium slag after the milling was shown in Fig. 1b, with the D_{50} of 32.7 μm and the D_{90} of 110 μm. Industrial-grade CO_2 and N_2 with a purity of 99.9% (v/v) were used to simulate the flue gas.

2.2 Preparation of Magnesium Slag Block

A certain mass of magnesium slag was weighed, 4% (mass fraction) of water was added, and it was rapidly stirred in a blender for 5 min, and then 145 g of the wet material was transferred to a stainless steel mold, and a specimen of 40 mm × 40 mm × 50 mm was prepared by keeping it under 20 MPa pressure for 1 min. After demolding, the samples were put into the carbonization kettle and cured at different conditions. The obtained specimens were named by the cured temperature and concentration, such as 25-10, which means that the specimen was cured at 25 ℃ and 10% CO_2 concentration. The

ISSN: 2414-1895 DOI: 10.6919/ICJE.202405_10(5).0039

specific curing conditions of different specimens are shown in Table 2. The carbonization kettle has a constant temperature heating function, which can simulate different temperatures of the kiln flue gas. The CO_2 and N_2 are proportionally mixed by a gas device with a CO_2 concentration of 10% (v/v) or 30% (v/v), and the gas mixture is introduced into the carbonization kettle through a pressure reducing valve. The pressure of the curing gas was 0.2 MPa, the time was set 1, 24 and 48 h, and the humidity was controlled at 50% by saturated calcium nitrate [22].

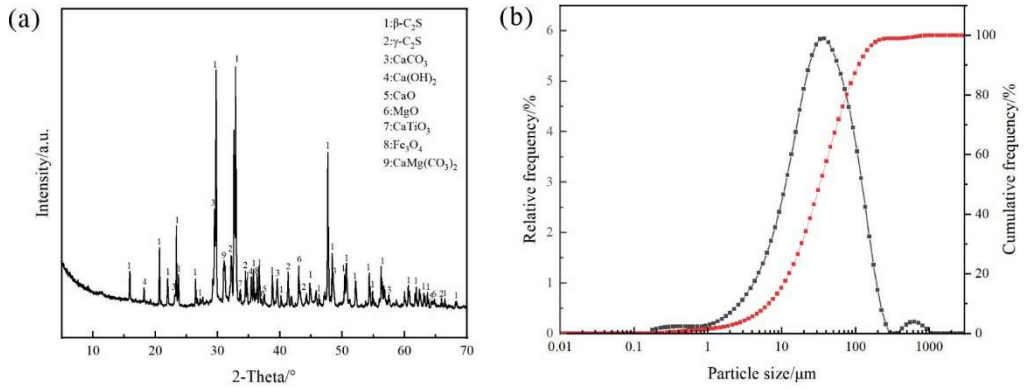

Fig. 1 (a) XRD pattern of magnesium slag, (b) particle size distribution of magnesium slag.

Table 1. Chemical composition of magnesium slag.

Composition	CaO	SiO_2	MgO	Fe_2O_3	Al_2O_3	Others
Mass fraction/%	63.05	25.82	4.21	3.58	1.34	2.00

Table 2. Curing conditions of magnesium slag block

Sample No.	Temperature / ℃	CO_2 concentration / %
25-10	25	10
40-10	40	10
60-10	60	10
80-10	80	10
120-10	120	10
25-30	25	30
40-30	40	30
60-30	60	30
80-30	80	30
120-30	120	30

2.3 Characterization

Compressive strength, water absorption and apparent density were determined according to Solid Concrete Bricks (GB/T 21144-2023). The compressive strength was measured by DYE-300S computerized automatic cement tester with the loading speed set at 0.5 mm/min. Each group of specimens was tested three times, and the average value and standard deviation were calculated. The chemical composition of the samples was analyzed by X-ray fluorescence spectrometer (XRF, Thermo Scientific ARL Perform'X). The phases of the raw material and specimens were characterized by an X-ray diffraction spectrometer (XRD, Smart Lab (9 kW), Rigaku), with scanning conditions of

ISSN: 2414-1895 DOI: 10.6919/ICJE.202405_10(5).0039

Cu Kα1 rays at a scanning rate of 10 °/min and a step rate of 0.02°/step. The data were collected from 5° to 70°. The samples were tested using a thermogravimetric differential thermal synchronous analyzer (STA8122, Rigaku) with a temperature range of 30~1000 ℃, a ramp rate of 10 ℃/min and a gas atmosphere of N_2. The particle size of the magnesium slag was characterized by an ultra-high-speed intelligent particle size distributor (Mastersizer 3000). The pore structure of the blocks was characterized by a low-field nuclear magnetic resonator (MesoMR12-060V). The morphology of the products was characterized by scanning electron microscopy (SEM, Merlin Compact) in secondary electron imaging mode with a test voltage of 10 kV.

3. Results and Discussion

3.1 Determination of Conservation Time

The effects of different curing temperatures and time on compressive strength at 10% and 30% CO_2 concentration are shown in Fig. 2a and b, respectively. It can be seen from Fig. 1 that all samples had an initial compressive strength after 1 h's curation. The compressive strength of the samples increased significantly when the curing time was extended to 24 h. Further extension of the curing time to 48 h, the compressive strength of the samples increased, but not minimally. Subsequent analyses were performed with the samples cured for 24 h. The same samples were used in later characterization.

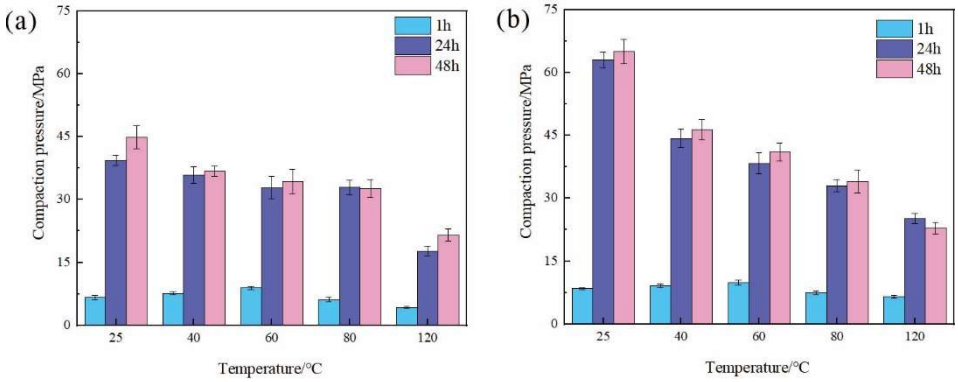

Fig. 2 Compressive strength of samples cured with (a) 10% and (b) 30% CO_2 concentration and different temperature and time

3.2 Compressive Strength Test

Taking the specimens cured for 24 h in Fig. 2 as an example, it can be seen that the compressive strength of magnesium slag specimens showed a gradual decrease with the increase of temperature. The compressive strength of the specimen 120-10 is 17.75 MPa, which is only 45.11% of that of specimen 25-10. The compressive strength of specimen 120-30 is only 25.13 MPa, the value is only 39.85% of that of specimen 25-30. The compressive strength of sample 120-30 was 25.13 MPa, the value was only 39.85% of that of sample 25-30. Research [23] shows that the increase in temperature accelerates the carbonization of C_2S and part of MgO and CaO in magnesium slag, which is manifested in the early stage of carbonation. There is a slight increase in the compressive strength oft he specimens, and as carbonization proceeds, the formation of carbonation products of calcium carbonate and silica gel on the periphery of the magnesium slag particles affecgts the continuous reaction of the un-carbonized mineral phases, which influences the compressive strength oft he specimens. On the other hand, the increase in temperature led to excessive volatilization of water inside the blocks and the reduction of the medium for CO_2 diffusion, which impeded the further carbonization [24]. Increasing the CO_2 concentration verified the above results, and Fig. 2 shows that at the same temperature, the compressive strength of magnesium slag specimens cured with 30% CO_2 concentration was greatly increased compared with that of 10%, with the greatest increase in the compressive strength of samples 25-30. The above analysis shows that the carbonization reaction of

ISSN: 2414-1895 DOI: 10.6919/ICJE.202405_10(5).0039

magnesium slag specimens is greatly affected by the curing temperature, and too high curing temperature will reduce the strength of magnesium slag specimens.

3.3 Water Absorption and Apparent Density

Fig. 3 shows the water absorption and apparent density of the specimens at different curing temperatures under 10% and 30% CO_2 concentrations, respectively. It can be seen from the figure that the water absorption of the cured specimens at both CO_2 concentrations increased gradually with increasing temperature, while the apparent density decreased gradually. This indicates that as the curing temperature increases, the content of carbonized products in the magnesium slag decreases and the densification of the specimens decreases. With the increase in temperature, the pore structure of the specimen becomes relatively loose and the water absorption increases, which corresponds to the decrease in compressive strength in terms of macromechanics. The above results show that the compressive strength and apparent density of the specimens at the curing temperature are inversely and directly proportional to the water absorption, respectively. When the curing temperature is 25 ℃, the water absorption of the specimens with 10% and 30% CO_2 concentration is 12.07% and 10.38%, respectively, and the apparent density is 2.64 and 2.69 g/cm^3, respectively. When the curing temperature is 60 ℃, the water absorption of the specimens with 10% and 30% CO_2 concentration is 12.81% and 12.25%, respectively, and the apparent density is 2.44 and 2.52 g/cm^3, respectively. It can be seen that when the curing temperature is low, increasing the CO_2 concentration helps to reduce the water absorption of the specimen and increase the apparent density of the specimen. When the curing temperature is high, increasing the CO_2 concentration has less effect on the water absorption and apparent density of the specimen.

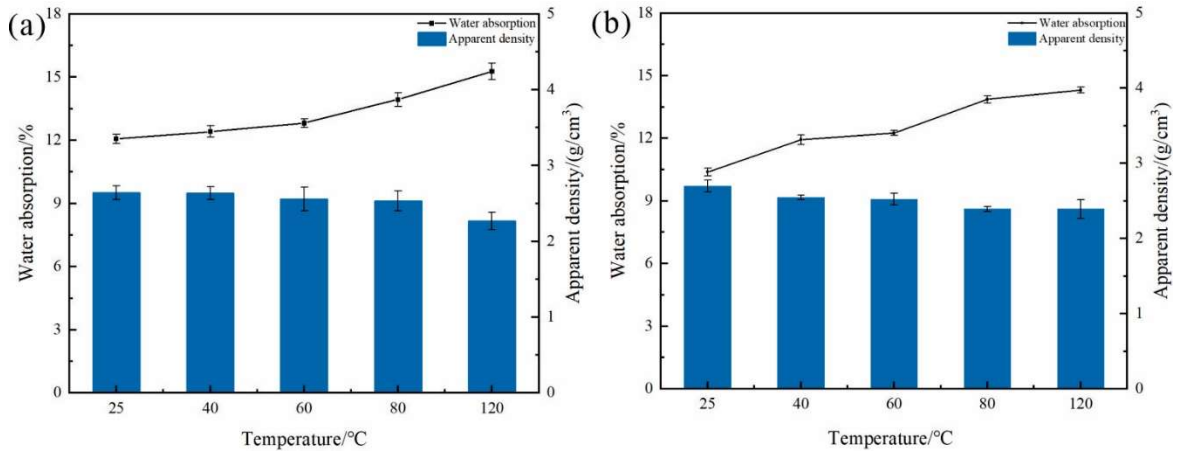

Fig. 3 Water absorption and apparent density of samples cured with (a)10% and (b) 30% CO_2 concentration

3.4 Phase Indentification

3.4.1 XRD

Fig. 4 shows the XRD patterns of the specimens cured at different temperatures at 10% and 30% CO_2 concentration, respectively. From the figure, it can be seen that the main change in phase composition of the specimens (see Fig. 1a) is reflected in the diffraction peaks of calcite, indicating that the carbonized products of magnesium slag are mainly calcite-type calcium carbonate. Meanwhile, the diffraction peak of $Ca(OH)_2$ (2θ = 18.22°) disappeared after carbonization, indicating that it participated in the reaction during the curing process. In the curing process, the diffraction peaks at 2θ = 29.72 ° and 2θ = 32.84 °, which are the characteristic peaks of β-C_2S, gradually increased with increasing curing temperature. However, the diffraction peak at 2θ = 29.48 ° showed a decreasing trend. The results show that the increase in temperature inhibits the carbonization reaction of β-C_2S.

The mineral phases of the specimens were quantitatively analyzed using 10% (mass fraction) ZnO as internal standard, and the results are shown in Table 3. It can be seen from Table 3 that with the

ISSN: 2414-1895 DOI: 10.6919/ICJE.202405_10(5).0039

increase of curing temperature, the C_2S content of sample 25-10 decreased by 6.04% compared to that of sample 120-10, and the C_2S content of sample 25-30 decreased by 7.56% compared to that of sample 120-30. Meanwhile, the content of calcite-type calcium carbonate in the amorphous phase increased in sample 25-10 and sample 120-10 compared to the samples prepared at high temperature.

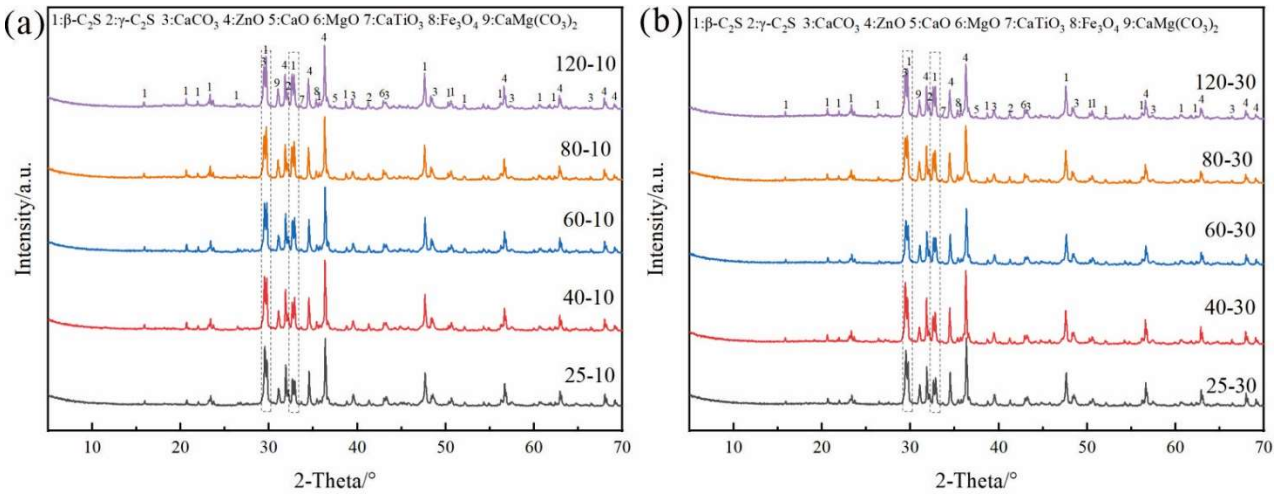

Fig. 4 XRD patterns of samples cured with (a) 10% and (b) 30% CO_2 concentration.

Table 3. Composition of samples prepared in different conditions.

Samples	Mass fraction/%						
	β-C_2S	γ-C_2S	$CaCO_3$	$CaMg(CO_3)_2$	MgO	Fe_3O_4	Others+Amorphous
25-10	20.22	5.56	25.56	4.00	1.33	0.67	42.67
25-30	19.33	4.00	27.89	5.56	1.44	0.56	41.22
120-10	26.56	5.22	21.78	4.44	1.78	0.67	39.67
120-30	26.89	5.33	24.78	4.67	2.00	0.67	35.78

3.4.2 TG-DTG

Fig. 5a and b show the TG and DTG curves for specimens cured at 10% CO_2 concentration, respectively. Fig. 5c and d show the TG and DTG curves of the specimens cured at 30% CO_2 concentration, respectively. From the DTG curves, it can be seen that there are three main decomposition peaks in the carbonized magnesium slag specimens, in which the decomposition near 100 and 375 ℃ is related to water in the silica gel with low and high crystallinity, respectively [20], and the decomposition at 400 ~ 675 ℃ is mainly attributed to the amorphous calcium carbonate and calcite with poor crystallinity. The decomposition at 675 ~ 850 ℃ is attributed to calcite with better crystallinity.

Combined with the change of DTG peak, the CO_2 mass loss of TG curve at 400 ~ 850 ℃ was calculated, and the specific results are shown in Table 4. As can be seen from Table 4, at the same CO_2 concentration, the decomposition amount of CO_2 in the specimen decreases with increasing temperature, while at the same curing temperature, the decomposition amount of CO_2 in the specimen increases gradually. The results of the thermal analysis TG-DTG and XRD are consistent with each other, which indicates that at the low concentration of CO_2 curing environment, the amount of CO_2 solidfied in the specimen decreases with increasing curing temperature, that is, the high temperature will inhibit the carbonization of magnesium slag.

ISSN: 2414-1895 DOI: 10.6919/ICJE.202405_10(5).0039

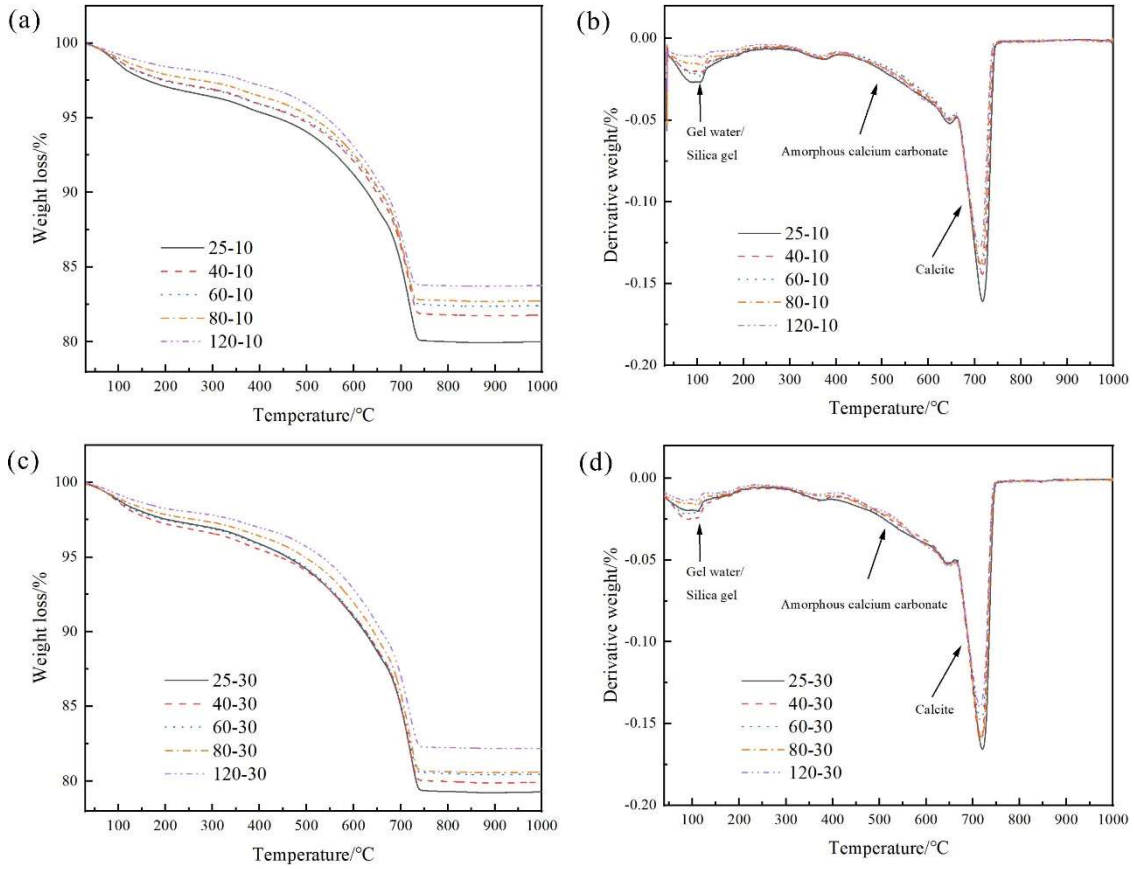

Fig. 5 TG and DTG curves of specimens cured at 10% CO_2 concentration (a and b) and 30% CO_2 concentration (c and d).

Table 4. Decomposition of CO_2 in specimens prepared in different conditions.

Sample No.	CO_2 weight loss/ %	Sample No.	CO_2 weight loss/ %
25-10	15.42	25-30	16.66
40-10	14.18	40-30	15.84
60-10	13.52	60-30	15.63
80-10	13.74	80-30	15.40
120-10	13.44	120-30	14.77

3.5 Microscopic Porosity

The transverse relaxed curves measured by low-field NMR were fitted to multi-exponential curves using Multi-Exp Inv Analysis software. The main products of magnesium slag are calcium carbonate and silica gel. According to Wang et al [25], the pore size distribution curves of the specimens cured at different temperatures and CO_2 concentrations were obtained (Fig. 6a and b). The total porosity of the specimens is shown in Table 5. From Fig. 6, it can be seen that the peaks of the pore distribution are mainly concentrated at 1 nm ~0.1 μm, 0.1-1 μm and 1-10 μm, respectively. According to previous studies, these pores can be categorized into micropores (1 nm - 0.1 μm), mesopores (0.1 - 1 μm) and macropores (1-10 μm) [26]. The pores in samples 25-10 and 25-30 were dominated by micropores and mesopores with fewer macropores. As the curing temperature increased, there was relatively little change in the pore size of micropores and mesopores in the specimen blocks, while the pore size and distribution of the macropores varied considerably. Among all the specimens, the specimen 120-10 had the highest distribution of macropores, and the total porosity increased by 4.16% compared tot he specimen 25-10. Combined with Table 5, it can be seen that the increase of temperature leads to

ISSN: 2414-1895 DOI: 10.6919/ICJE.202405_10(5).0039

the increase of porosity in the specimens, especially the increase of macroporosity content. Combined with the pore distribution and pore size, it can be seen that an increase in temperature inhibits the carbonization of mineral phases such as C_2S in the magnesium slag and reduces the filling of pores by carbonized products, which leads to a relatively loose pore structure. In the macroscopic level, it corresponds to the decrease in the compressive strength of the specimen and the increase in water absorption.

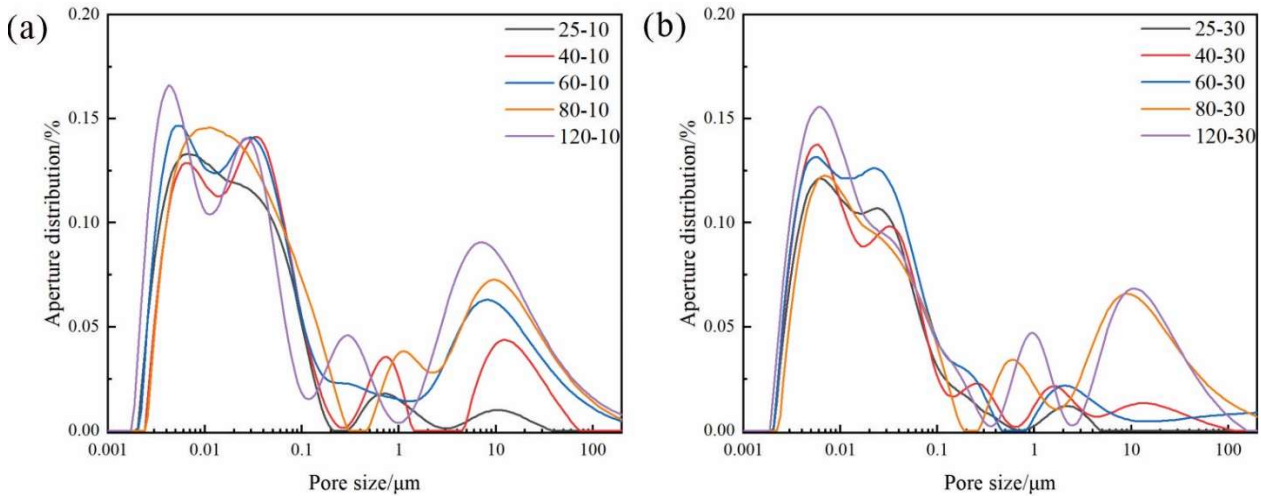

Fig. 6 Pore size distribution of specimens cured at (a) 10% CO_2 and (b) 30% CO_2 concentration.

Table 5. Total porosity of the specimen blocks.

Sample No.	Total porosity / %	Sample No.	Total porosity / %
25-10	11.40	25-30	9.46
40-10	13.08	40-30	10.76
60-10	16.74	60-30	12.16
80-10	17.18	80-30	13.60
120-10	18.34	120-30	15.34

3.6 Microstructures

Figure 7 shows the SEM images of the specimen blocks cured at 10% and 30% CO_2 concentration, respectively. It can be seen from the figure that the microstructure of the blocks change from dense to loose with the increasing curing temperature, the carbonized products on the surface of the specimens decreases gradually. From Fig. 7a and b, it can be seen that the area of carbonizd products on the surface of the specimen 25- 10 increased significantly with the increase of CO_2 concentration than that of specimen 25-30. When the curing temperature was increased to 80 ℃, the carbonized products on the surface of the specimen were relatively decreased, and the micro-morphology of the specimen did not change significantly as the CO_2 concentration was increased (Fig. 7c and d). When the curing temperature was further increased to 120 ℃, more pores appeared between the particles of 120-10 and 120-30 specimens, and the bonding state between the particles deteriorated, as well as the morphological shape of the calcium carbonate deteriorated, and the morphology of two samples differed greatly (Fig. 7e and f). Combined with the mechanical properties, phases and microstructure changes of the specimens, it can be seen that the increase in temperature will reduce the degree of carbonization of the blocks, increase the porosity betweenparticles, reduce the density of the specimen block, which leads to a decrease in the mechanical properties of the specimen blocks.

ISSN: 2414-1895 DOI: 10.6919/ICJE.202405_10(5).0039

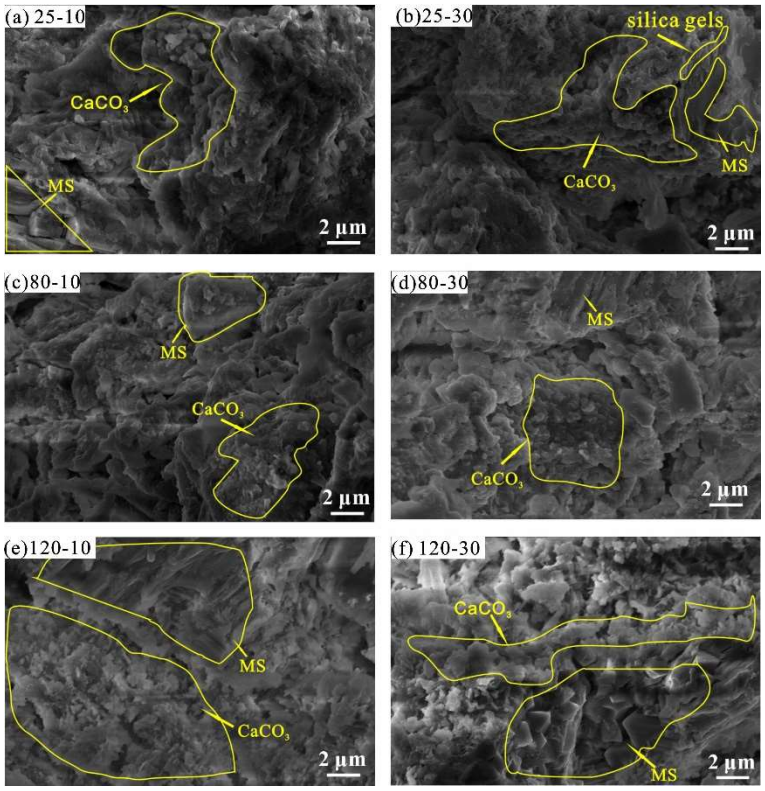

Fig. 7 SEM images of specimens cured at different conditions.

4. Conclusion

In this paper, the effects of CO_2 concentration and curing temperature on the carbonization of magnesium slag were systematically investigated by simulating industrial flue gas, and the following conclusions were drawn:

(1) The mechanical properties of magnesium slag specimens were obviously affected by the curing temperature. For specimens cured with 10% CO_2 concentration, the compressive strength of the specimen cured at 120 ℃ was 17.75 MPa, which was only 45.11% of that cured at 25 ℃. For the specimen cured at 25 ℃, the mechanical properties of specimens were more influenced by the CO_2 concentration, and the compressive strength of the specimens cured at 30% CO_2 concentration was as high as 63.06 MPa, which was 60.23% higher than that of the specimen cured at 10% CO_2 concentration. The effect of CO_2 concentration on the mechanical properties of the specimens decreased with the increase of curing temperature.

(2) With the increase of the curing temperature, the unreacted β-C_2S in the magnesium slag increased, and the carbonized products decreased. The effect of CO_2 concentration on the phases of the specimens was small, and the differences of each component was also small.

(3) The porosity of specimens increased with the increase of curing temperature, which was mainly reflected in the increase of the proportion of large pores. The increase of CO_2 concentration reduced the porosity and improved the densification as well as the mechanical properties of the specimens.

(4) The curing temperature also had a significant effect on the micro-morphology of the specimen. More carbonized products were formed between particles in specimens cured at room temperature. The products gradually decreased as the curing temperature increased.

Acknowledgments

This work was supported by National Natural Science Foundation of China (no. U1905216).

ISSN: 2414-1895 DOI: 10.6919/ICJE.202405_10(5).0039

References

[1] RAMAKRISHNAN S, KOLTUN P. Global warming impact of the magnesium produced in China using the Pidgeon process[J]. Resources, Conservation and Recycling, 2004, 42(1): 49-64.

[2] Yang X., Dong F., Zhang X., et al. Review on comprehensive utilization of magnesium slag and development prospect of preparing backfilling materials[J]. Minerals, 2022, 12(11): 1415.

[3] Jia L, Fan B., Huo R., et al. Study on quenching hydration reaction kinetics and desulfurization characteristics of magnesium slag[J]. Journal of Cleaner Production, 2018, 190: 12-23.

[4] Meng L, Wang Z, Guo Z. Effective separation of fusing agent from refined magnesium slag by supergravity technology[J]. Chemical Engineering and Processing - Process Intensification, 2022, 175: 108915.

[5] Tian Y, Wang L , Yang B, et al. Comparative evaluation of energy and resource consumption for vacuum carbothermal reduction and Pidgeon process used in magnesium production[J]. Journal of Magnesium and Alloys, 2022, 10(3): 697-706.

[6] AMINI O, GHASEMI M. Laboratory study of the effects of using magnesium slag on the geotechnical properties of cement stabilized soil[J]. Construction and Building Materials, 2019, 223: 409-420.

[7] Jing H, Zhang J, Gao M, et al. Base performances of cement-stabilized magnesium slag–aeolian sand mixture[J]. Acta Montanistica Slovaca, 2021(26): 427-443.

[8] Fan B., Jia L, Li B, et al. Study on desulfurization performances of magnesium slag with different hydration modification[J]. Journal of Material Cycles and Waste Management, 2018, 20(3): 1771-1780.

[9] Fan B, Jia L, Han F, et al. Study on magnesium slag desulfurizer modified by additives in quenching hydration[J]. Journal of Material Cycles and Waste Management, 2019, 21(5): 1211-1223.

[10] Liu L, Ding X, TU B, et al. Energy evolution and mechanical properties of modified magnesium slag-based backfill materials at different curing temperatures[J]. Construction and Building Materials, 2024, 411: 134555.

[11] Xxie G, Liu L, Suo Y, et al. High-value utilization of modified magnesium slag solid waste and its application as a low-carbon cement admixture[J]. Journal of Environmental Management, 2024, 349: 119551.

[12] Ruan S, Liu L, Xie L, et al. Mechanical properties and leaching behavior of modified magnesium slag cemented aeolian sand paste backfill materials[J]. Construction and Building Materials, 2023, 387: 131641.

[13] Li H , Huang Y, Yang J, et al. Approach to the management of magnesium slag via the production of Portland cement clinker[J]. Journal of Material Cycles and Waste Management, 2018, 20(3): 1701-1709.

[14] Ji G , Peng X , Wang S , et al. Influence of magnesium slag as a mineral admixture on the performance of concrete[J]. Construction and Building Materials, 2021, 295: 123619.

[15] Mo L, Hao , Liu Y , et al. Preparation of calcium carbonate binders via CO2 activation of magnesium slag[J]. Cement and Concrete Research, 2019, 121: 81-90.

[16] Zhong D, Zhang W, ZHANG S W, et al. Preparation of aragonite whisker-rich materials by wet carbonation of magnesium slag: a sustainable approach for CO2 sequestration and reinforced cement[J]. Construction and Building Materials, 2024, 418: 135429.

[17] Gao M, Dai J, Jing H, et al. Investigation of the performance of cement-stabilized magnesium slag as a road base material[J]. Construction and Building Materials, 2023, 403: 133065.

[18] Lei M, Deng S, Huang K, et al. Preparation and characterization of a CO2 activated aerated concrete with magnesium slag as carbonatable binder[J]. Construction and Building Materials, 2022, 353: 129112.

[19] Lei , Yu H, Feng P, et al. Flue gas carbonation curing of steel slag blocks: effects of residual heat and water vapor[J]. Construction and Building Materials, 2023, 384: 131330.

[20] Zhang C, Liu S , Tang P, et al. Enhancing the hardening properties and microstructure of magnesium slag blocks by carbonation-hydration sequential curing[J]. Journal of Building Engineering, 2023, 76: 107414.

[21] Xie D M, Zhang Z, Liu Z, et al. Utilization of magnesium slag to prepare CO2 solidified fiber cement board[J]. Construction and Building Materials, 2024, 411: 134345.

[22] Mu Y, Liu Z, WANG F. Carbonation kinetics of γ-dicalcium silicate[J]. Journal of the Chinese Ceramic Society, 2022, 50(2): 457-465 (in Chinese).

ISSN: 2414-1895 DOI: 10.6919/ICJE.202405_10(5).0039

[23] Guan X, Liu S H, Feng C, et al. The hardening behavior of γ-C2S binder using accelerated carbonation[J]. Construction and Building Materials, 2016, 114: 204-207.

[24] Liu Z, Lv C, Wang F, et al. Recent advances in carbonatable binders[J]. Cement and Concrete Research, 2023, 173: 107286.

[25] Jiang Y, LI L, Lu J, et al. Enhancing the microstructure and surface texture of recycled concrete fine aggregate via magnesium-modified carbonation[J]. Cement and Concrete Research, 2022, 162: 106967.

[26] Han X, Wang B, Feng J. Relationship between fractal feature and compressive strength of concrete based on MIP[J]. Construction and Building Materials, 2022, 322: 126504.